Crystallographic Properties and Elemental Migration in two-stage prepared $CuIn_{1-x}Al_xSe_2$ thin films for photovoltaic applications

Rémi Aninat[a+], Guillaume Zoppi[a]*, Agnès Tempez[b], Patrick Chapon[b], Neil S. Beattie[a], Robert Miles[a] and Ian Forbes[a]

[a] *Northumbria Photovoltaics Applications Centre, Northumbria University, Ellison Building, Newcastle upon Tyne, NE1 8ST, UK.*

[b] *Horiba Jobin Yvon SAS, Avenue de la Vauve, Passage Jobin Yvon, CS 45002 - 91120 Palaiseau, France.*

**Corresponding author. E-mail: guillaume.zoppi@northumbria.ac.uk*

[+] Now at: Département Sciences et Analyse des Matériaux, Centre de Recherche Public - Gabriel Lippmann, 41, rue du Brill, L-4422 Belvaux, Luxembourg

Keywords

A. Thin films; semiconductors; B. vapour deposition; D. X-ray diffraction

Abstract

Two-stage fabrication of $CuIn_{1-x}Al_xSe_2$ thin films for photovoltaic absorbers using sputtered Cu-In-Al metallic precursors has been investigated. Precursors containing different relative amounts of Al were selenised and their structural and chemical properties characterised. X-ray diffraction (XRD) analyses revealed that the Al was only incorporated into the chalcopyrite structure for precursor composition ratios x=[Al]/([Al]+[In])≥0.38, while chemical analysis of the cross-section indicated partial segregation of Al near the back of the film. Precursor films in the range of compositions that yielded no Al incorporation were then selenised at four different temperatures. Glow discharge optical emission spectroscopy, plasma profiling time-of-flight mass spectrometry and XRD analyses provided an insight into the diffusion processes and reactions taking place during the selenisation stage. The effect of post-selenisation annealing without additional Se was also investigated, and led to partial incorporation of the Al into the $CuInSe_2$ lattice but no rediffusion.

1 Introduction

The most efficient thin-film solar cells to date, with a record efficiency of 20.3±0.6% [1], are based on a $CuIn_{1-x}Ga_xSe_2$ (CIGS) absorber layer. $CuIn_{1-x}Ga_xSe_2$, like $CuInSe_2$ (CIS), is chalcopyrite, with Ga substituting In in the ratio x=[Ga]/([Ga]+[In]). This ratio can be altered to tune the band gap between that of $CuInSe_2$ (CIS), 1.0 eV, and that of $CuGaSe_2$ (CGS), 1.7 eV [2, 3]. In an ideal device, a band gap increase yields, in terms of current-voltage (I-V) characteristics, an increase of the open-circuit voltage (V_{OC}) and a parallel decrease of the

short-circuit current (I_{SC}). As a result there exists an optimal band gap for single junction devices, representing the best trade-off between V_{OC} and I_{SC}. According to detailed balance calculations, and because of the specific bands of absorption of the solar spectrum in the atmosphere, two band gaps actually yield almost equal optimal efficiencies under air mass 1.5 illumination: 1.15 eV, with 32.8% efficiency, and 1.35 eV, with 33.0% efficiency [4]. In CIGS devices, the V_{OC} increase with band gap becomes less pronounced for x>0.3, due to increasing defect concentrations [5]. This x=0.3 ratio corresponds, if the Ga distribution is uniform, to a band gap of ≈1.2 eV [3]. For this reason, the best performing solar devices are made with the nearest optimal (effective) band gap E_G≈1.15 eV [6, 7]. However, being able to reach the higher band gap optimum without V_{OC} degradation would help to reduce resistive losses in solar cells, and even more so in modules, where the current has to be transported over greater distances and where cell interconnects are present [2]. An alternative to CIGS is $CuIn_{1-x}Al_xSe_2$ (CIAS), obtained by replacing Ga by Al. The CIAS band gap is tuneable over a much wider range than CIGS: from 1.0 eV for CIS to 2.7 eV for $CuAlSe_2$ (CAS). CIAS devices of efficiencies up to 16.9% have been obtained by Marsillac *et al.* by co-evaporation [8]. This latter device performed 0.4% better than an equivalent CIGS device of identical band gap (1.15 eV) built along with it, which suggests reduced losses in CIAS. Several specificities of CIAS might explain this result. Among them, the fact that less Al is required in CIAS to reach a given band gap than the amount of Ga necessary to reach the same band gap in CIGS. Furthermore, since both $CuAlSe_2$ and $CuGaSe_2$ have similar lattice parameters [9, 10] then, according to Vegard's law, CIAS films with identical band gap to CIGS can be fabricated with less lattice strain, compared to the lattice of $CuInSe_2$. By reducing the lattice strain, less crystal defects (e.g. dislocations) are likely to form.
CIAS could therefore find applications in single junction solar devices (i.e. to reach 1.35 eV with reduced losses) as well as in tandem or multi-junction devices, where the different combinations of band gaps identified as optimum can be reached. For this work, the so-called two-stage process was chosen over co-evaporation because it is easier to scale-up and yields equivalent or higher efficiencies for CIGS devices at the module scale [11]. In this article, we present the crystallographic properties of CIAS thin films produced by selenisation of sputtered metallic precursors as a function of metallic precursor composition and selenisation conditions.

2 Experimental

Cu-In-Al metallic precursors were sputter-deposited on a soda lime glass (SLG) substrate coated with an 850 nm thick Mo back contact layer. A Nordiko 2000 radio frequency (RF) magnetron sputtering system with elemental targets was used for depositing the back contact and the metallic precursors. The system geometry was set up for sequential deposition. The substrates were continuously rotated (5 rpm) underneath the targets so as to deposit a succession of very thin (≈1 nm thick) elemental layers.

The metallic precursor thicknesses, as measured by stylus profilometry, were in the range 1100±200 nm for the samples of section 3.1 and ≈650±60 nm for those of section 3.2. An additional 100 nm thick Cu capping layer was deposited on top of the precursors of section 3.2 because it has been reported to limit the oxidation of the Al [12]. After selenisation, the thicknesses for the samples grown in both sections 3.1 and 3.2 were in the range 2.4-2.6 µm and 2.0-2.3µm, respectively. Note that the error on the thickness measurements was due to a high surface roughness on as-deposited precursors. This phenomenon is due to In "islands" protruding from the surface (see reference [13] for more details). These islands were already reported to form in Cu-In precursors for [In]/[Cu]>2 by Chung *et al.* [8]. They were systematically observed in the precursors produced in our setup when both In and Al were present.

Elemental Se was thermally evaporated on the metallic precursors in a K. J. Lesker Nano38 system, and the films were subsequently annealed in a 3-zone large bore Carbolite GHC 12/450 tube furnace. Samples were loaded in a quartz tube and pumped down to ≈0.1 Pa before injecting a pure atmosphere of Ar or H_2/N_2 prior to the annealing process. The thickness of the selenium was varied between 2.2 µm and 3.0 µm, depending on the precursor thickness, to allow full conversion of the precursor into CIAS. Imaging of the cross-section was performed in a FEI Quanta 200 secondary electron microscope (SEM). The chemical properties of the bulk were characterised by energy dispersive (EDS) or wavelength dispersive (WDS) X-ray spectroscopy with Oxford Instruments INCA ENERGY or INCA WAVE spectrometers, respectively. Note that EDS compositions were affected by partial overlapping of the Al K series and the Se L series when these two elements were present. Indeed, the energy difference between the two series is less than 90 eV, lower than the 133 eV limit of resolution of the instrument. The error resulting from this partial overlap was not precisely quantified, but must be bore in mind for the interpretation of the data from Table 3. WDS, on the other hand, offers a much higher resolution (typically 5 eV) and can resolve the

Al K series and Se L series. This is the reason why it was used for the detection of these two elements in section 3.1, in parallel with EDS for the remaining elements. However, quantitative analysis with WDS requires prior calibration, for which the appropriate calibration standards were not available to us. Therefore, the results of the WDS/EDS experiment on A3' (Figure 4) were only qualitative. For clarity, the ratios x=[Al]/([Al]+[In]) are noted x_p, x_s and x_{xrd} depending on whether they were measured on the as-deposited precursor, on the selenised sample or calculated from the X-ray diffraction (XRD) data, respectively.

The structural properties were analysed by XRD in a Brüker D5000 diffractometer. The chemical depth profiles were measured in two Horiba Scientific instruments using glow discharge-based techniques: a Plasma Profiling Time-of-Flight Mass Spectrometer (PP-TOFMS) and a GD- Profiler 2 Glow Discharge Optical Emission Spectrometer (GD-OES). These two techniques have low matrix effects and average the signal over large areas to reduce the effect of local features or inhomegeneities. Deposition and processing data for the samples of this article are summarised in Table 1.

3 Results and discussions

3.1 Impact of precursor composition on the level of alloying with Al

The effect of altering the x_p=[Al]/([Al]+[In]) ratio, as measured in the metallic precursors, was tested on four samples selenised in similar conditions. A1, A2 and A3 were selenised at 530°C under 1000 Pa of H_2/N_2 and A4 at 540 °C under 1000 Pa of Ar. Note that selenisation trials under Ar and H_2/N_2 atmospheres have been compared and led to no obvious variation, so that the change from one to the other is considered as neutral. The difference in selenisation temperature between A1-A3 (530°C) and A4 (540°C), on the other hand, could have induced some limited variation, so that A4 is included for qualitative comparison only. The XRD results for the selenised samples are reported in Figure 1.

The composition ratios x=0.11 (A1) and x_p=0.27 (A2) did not yield any incorporation of the aluminium into the CIS (PDF 01-078-2001) lattice, and the element was not present in any detectable crystalline form. For x_p =0.38 (A3), however, Al-incorporation was observed. The pattern of this sample reveals several broad, overlapping peaks, which remained after potassium cyanide etching, indicating that they belong to multiple $CuIn_{1-x}Al_xSe_2$ phases (with different x values) and not to $Cu_{2-x}Se$ [14]. At x_p =0.51 (A4), also, some CIAS was observed, although only as traces, and In-free CAS (PDF 00-044-1269) was detected. The

presence of CAS is implied from the relative increase in the intensity and area of the peak normally assigned to CIS (103), in comparison to the CIS (112) peak. The level of incorporation of aluminium observed in A3 was shown to vary from sample to sample. A3', consisting of the same metallic precursor and selenised together with A3, also showed some incorporation of Al, but the XRD pattern suggests a different distribution of this incorporation (Figure 2). In particular, some Al seems to have segregated completely from the In, causing the formation of a $CuAlSe_2$ phase (PDF 00-044-1269).

GD-OES was performed on sample A3 and the depth profiles are presented in Figure 3. A certain depth of film is removed at each sputtering cycle, so that the x-axis ("sputtering time") can be associated with the depth into the sample. t=0 s therefore corresponds to the film upper surface, while the drop of all but Mo signal for t>250s indicates that the interface of the film with the back contact has been reached. The Al signal has a maximum in region *a* and then a dip and a gradual increase towards the back (region *b*). Indium is depleted in region *a* and follows a reverse trend to Al in region *b*, with a decreasing gradient towards the back contact. Cu and Se are maximum at the surface and evenly distributed throughout the bulk. Oxygen (not shown) also increases at the surface and is almost absent from region *b*. The interface with the back contact (180 s<t<250 s) is believed to be relatively rough, so that throughout region *c*, depth resolution is partially lost. Some comments can however be made on this region. First of all, the In signal decreases from 210 s, while the Al signal stays stable. All the film elements except Se then drastically decrease at the end of region *c*, indicating that the back contact is fully reached. Region *c* is interpreted as an interfacial layer, more Al-rich than the rest of the bulk, associated with the most shifted (112) reflections of the XRD. Note also that the Se signal slumps only beyond the border of region *c* (t=270 s), which indicates the presence of a $MoSe_2$ layer at the interface film-Mo, also detected at the relevant detection angles of the XRD pattern (not shown).

Combined EDS and WDS analyses were carried out along the cross-section of A3', in order to correlate the elemental distribution with particular features observed in the SEM micrograph (Figure 4). Al and Se were detected by WDS, while Cu, In and Mo were analysed by EDS. The micrograph indicates the presence of two layers on top of the Mo film, with a small Al-rich layer at the bottom and an In-rich top layer. This observation matches the XRD analysis of A3' in Figure 2, where CIS, graded CIAS and CAS phases were detected. This phenomenon is similar to that of two-stage processed CIGS, as described in [15].

The XRD analysis implies that no incorporation of Al into the CIS lattice or any other crystalline phase takes place for compositions below x_p =0.38. At x_p =0.38, although some CIAS forms, it is not single phase (i.e. one single x value throughout), but instead shows graded compositions of Al and In, leading to partial phase segregation. The distribution observed (GD-OES, XRD) also varies from one sample to the next (e.g. A3, A3'), for no discernable reason. A similar lack of incorporation for x_p<0.39 was reported in [16]. Cross section WDS and EDS shows that the incorporation of Al into the chalcopyrite lattice yields smaller grain size, which coincides with the poorer crystallinity (broader peaks) observed for the CIAS phases by XRD. It is unclear whether the different CIAS phases are a result of the sole depth distribution of the elements Al and In, or if they also result from variable degrees of incorporation of Al, or even non-homogeneous lateral distribution. At x_p =0.51 (sample A4), finally, almost complete segregation between CIS and CAS was observed, with CIAS phases of very low crystallinity only.

3.2 Impact of the maximum selenisation temperature

In order to understand the causes preventing the incorporation of Al into CIS in low x value samples, selenisation trials at different maximum temperatures were performed on x_p =0.11 precursors. Cu-In-Al/Cu samples were selenised in the tube furnace at four different maximum temperatures, 250°C, 350°C, 450°C and 530°C. Two additional low temperature steps at 130ºC and 250ºC (for the 350 ºC, 450 ºC and 530ºC samples) were introduced because those steps were reported in [17] to yield good crystallinity in CIS grown from stacked elemental layers. The precursor bulks were of atomic composition 50.2% Cu, 44.3% In and 5.5% Al before capping. A 100 nm thick Cu layer ("cap") was added at the end of the sequence, yielding the Cu-rich composition reported in Table 1.

The XRD patterns of the selenised samples are shown in Figure 5. The crystalline phases identified and the annealing temperature steps applied are summarized in Table 2. They show the presence of $Cu_{2-x}Se$ (powder diffraction file PDF 00-006-0680), $Cu_{0.938}InSe_2$ (PDF 01-078-2001) and trace $Cu_{16}In_9$ (PDF 00-026-0523) in all selenised samples. $Cu_{16}In_9$ indicates that small amount of metallic precursor remained unconverted. In sample B1, $CuSe_2$ (PDF 01-071-0046) and In_4Se_3 (PDF 01-083-0039) were also detected. The CIS formed was of low crystallinity at this temperature. The pattern also reveals the presence of small α-In_2Se_3 and elemental In phases, which indicates that the precursor has only been partially converted, and is typical of this low temperature.

In sample B2, In_4Se_3 and $CuSe_2$ reflections have disappeared, while CIS (PDF 01-078-2001) has grown and become more crystalline, and $Cu_{2-x}Se$ and some In reflections remain present. The same phases were observed at 450°C (sample B3), and finally only CIS and $Cu_{2-x}Se$ were visible at 540°C (sample B4). No Al-containing phase was observed in any of these samples.

The EDS analyses are shown in Table 3. Note that the ratio [Se]/([Al]+[In]) rather than [Se]/([Cu]+[In]+[Al]) is used as a figure of merit in Table 3 to determine whether Se is in excess or in deficit for the formation of $CuIn_{1-x}Al_xSe_2$. This ratio was chosen due to the fact that Cu is in large excess in the precursor, and the element III (Al or In) is therefore the limiting reactant, compared to Cu, for the reaction of formation of $CuIn_{1-x}Al_xSe_2$. Thus stoichiometric condition is fulfilled for [Se]/([Al]+[In])=2.The oxygen reaches a maximum of 6.2 at% at 540°C (B4). Note however that the composition of this last sample was only measured after a post-selenisation anneal at 573°C (discussed in section 3.3) and therefore higher levels of oxygen are expected. The measured composition is very Cu- and Se-rich at 250°C (B1), with [Cu]/([Al]+[In])≈6.09 (≈1.63 in as-deposited film) and [Se]/([In]+[Al])≈14.33 (2.00 for stoichiometry). This is attributed to an increased presence of these elements near the surface (Cu cap layer and Se evaporated layer), causing an increased X-ray signal in comparison to the other elements buried deeper in the bulk. At 350°C (B2), [Cu]/([Al]+[In])≈1.65, which is close to the calculated Cu-rich composition of the as-deposited precursor, 1.63. At 450°C (B3), [Cu]/([In]+[Al])≈1.02 is lower than in the as-deposited precursor, while x_s = [Al]/([Al]+[In])≈0.09 is comparable with the as-deposited composition.

At 540°C (B4), [Cu]/([In]+[Al]) increases slightly to 1.14 and [Se]/([In]+[Al]) decreases once more (1.72), so that the overall composition appears Cu-rich and more Se-deficient than at 450°C.

The four B samples were analysed by PP-TOFMS and the resulting depth profiles are shown in Figure 6. Details on the setup can be found in [18]. Depth profiles are displayed as ion beam ratios (IBR). The IBR is the ratio between the signal of a peak, corrected for the isotopic abundance, and the sum of ion matrix signals, corrected each for isotopic abundance. Here $^{27}Al^+$, $^{63}Cu^+$, $^{82}Se^+$, $^{98}Mo^+$, and $^{115}In^+$ are used as matrix ions.

In sample B1, the indium is absent from region *a*, but has a local maximum in region *b* and has a plateau in region *c*. The Se signal is maximum in region *a* and decreases towards the back. The Cu signal has a plateau in region *a*, an important notch in region *b* and a sloped profile in region ***c***. Most remarkable is the aggregation of the Al at the back of the film,

already at 250°C. In comparison, sample B2 shows an enhanced interdiffusion of all the elements with the exception of Al, which remains at the back. Region *a* is depleted in Cu but contains a local maximum for In, while region *b* is depleted in In and contains a local maximum for Cu. The notch in the Cu profile is no longer present. In sample B3, Cu, In and Se are distributed fairly evenly. Finally, the depth profile of sample B4 is very similar to that of sample B3 for all the elements. The noise in all the signals of B4 is attributed to extended roughness, due possibly to pinholes in the Mo. This is supported by the rise the rise of the Mo signal prior to that of Al on the inset of sample B4.

Two of the known formation pathways for CIS reported in the literature [19] can apply to this work:

$CuSe+InSe \rightarrow CuInSe_2$ **(1)**

$Cu_2Se+2InSe+Se \rightarrow 2CuInSe_2$ **(2)**

Reaction (1) starts at the melting point of Se, 221°C, with the formation of the binary selenides $CuSe_2$ and In_4Se_3 and is relatively slow. CuSe and InSe can be formed via:

$CuSe_2+In_4Se_3 \rightarrow CuSe+4InSe$ **(3)**

Reaction (2) starts at 380°C, and is faster than (1) [19]. It proceeds via the intermediary reaction:

$2CuSe \rightarrow Cu_2Se+Se$ **(4)**

These reactions can be matched to the XRD patterns and the PP-TOFMS depth profiles in order to gain understanding of the trends observed.

In sample B1 (250°C), Se and the Cu cap have only partially diffused into the bulk (PP-TOFMS, EDS), leading to $CuSe_2$ and $Cu_{2-x}Se$ phases being present in region *a* (Figure 6). In_4Se_3 is present in region *b*, and formed from the In islands mentioned in section 2, normally present at the bulk surface, but buried in this case underneath the Cu cap. Only reaction (1) can account for the presence of CIS in this sample. The high presence of In_4Se_3 and $CuSe_2$ in spite of the long selenisation process (30 min dwell at 250°C), indicate that reaction (3) (and consequently (1)) was blocked. This is attributed to the formation of large crystallites of either $CuSe_2$ or In_4Se_3 (reactant of InSe), which can have resulted from the slow ramping rate applied in the tube furnace (≈18°C/min). Large crystallite size was also reported in [19] to impede the formation of CIS. In sample B2 (350°C), the CIS phase shows an important growth resulting from the total consumption of $CuSe_2$ and In_4Se_3, to form CIS. This was made possible by the peritectic decomposition of $CuSe_2$ into CuSe and a Se melt at 340°C, to form CIS via (1). A better penetration of the Se from the front into the bulk was certainly another factor in this growth. Copper selenides are also present at the surface, with possibly a

thin In phase underneath (PP-TOFMS, XRD). In sample B3 (450°C), the maximum temperature was high enough to consume some of the Cu_2Se (high temperature form of $Cu_{2-x}Se$) to form CIS via reaction (2). This is supported by the dampening of the (111) $Cu_{2-x}Se$ reflection the most shifted towards higher 2θ angles and the slight growth of the CIS phase compared to B2. Sample B4 (540°C) is very similar to B3.The absence of Al from the XRD phases suggests that it must be present as amorphous Al or Al_2O_3. Al_2O_3 in particular is known to form very easily and fast [20] at the surface of Al-containing alloys. A crystalline form of Al_2O_3 was detected at the back of CIAS films by Dwyer *et al.*[12], but was not detected here.

Depth profiles show that the segregation of Al at the back has already taken place at 250°C (sample B1). This phenomenon is very similar to the observed segregation of Ga at the back of two-stage processed CIGS [21]. The most commonly suggested reason for this phenomenon is the relatively high temperature of formation of Ga selenides, compared to In selenides [21, 22]. This hypothesis also applies to CIAS, since the only known selenide of aluminium is Al_2Se_3, which was reported to form at 480°C [23], against 221°C for the first In selenides. At the melting point of Se, In and Cu are driven towards the front by the formation of selenides with the liquid Se which started diffusing, while Al stays at the back since it cannot form any selenide. As the temperature increases, the binary selenides of In and Cu then go on to forming CIS, and the Al stays at the back until 480°C, when it start forming CIAS and/or CAS [23]. At this stage, only interdiffusion between the CIS at the front and the CAS (or low In-content CIAS) at the back can yield a single phase CIAS bulk. This interdiffusion clearly did not occur in the selenised samples.

3.3 Post-selenisation anneal (PSA)

An additional annealing process of 60 min at 573°C, in a 1000 Pa Ar atmosphere and without introducing extra Se, was performed on B4. This sample had already been selenised at 540°C (see section 3.2). This treatment, to which we will refer in this discussion as post-selenisation anneal (PSA), was reported by Marudachalam *et al.* [21] to yield rediffusion of the Ga that had segregated at the back of 2-stage processed CIGS.

The XRD pattern of B4 after the treatment is displayed in Figure 7. It shows a modified CIS phase which peaks are broader and shifted towards higher angles. In spite of the relatively high temperature used, no bending or corrugation of the substrate was observed. The main diffraction peak of the Mo layer underlying the film, shown in the inset of Figure 7, did not shift more than the step size of the scan (<0.02°), unlike what would be expected if important

stresses were present in the sample. Furthermore, a small (112) CIS reflection is still present at the same angle as before PSA. The shifted reflections observed are therefore interpreted as a result of the incorporation of Al into the CIS lattice to form CIAS.

The lattice parameters *a* and *c* were assessed by fitting the experimental pattern with a tetragonal system of appropriate lattice parameters *a* and *c*. The main source of error in the lattice parameters was the step size of the scan, 0.02°. Since a change in *a* (or *c*) impacts differently the position of each peak of the pattern, the error in the lattice parameters depends on what peak is used for its determination. In this work, the (312) peak was used for assessing *a*, and the (116) peak for assessing *c*, yielding errors of ±0.002Å and ±0.005Å in *a* and *c* respectively, except for the CIS phase after PSA, where the (112) reflection was used for *a* due to a too low intensity of the (312) reflection. The lattice parameters before and after PSA, their respective errors and the calculated tetragonal distortion $\Delta=2-c/a$ are summarized in Table 4.

Using the change in lattice parameter *a* before PSA (CIS phase) and after PSA (CIAS phase) and assuming a Vegard's law, an estimate of the ratio x_{xrd}=[Al]/([Al]+[In]) can be calculated:

$$x_{xrd} = \frac{a(CuIn_{1-x}Al_xSe_2) - a(CuInSe_2)}{a(CuAlSe_2) - a(CuInSe_2)} \quad \textbf{(5)}$$

with *a(M)* the lattice parameter of the species *M*. The values used to calculate x_{xrd} are *a*($CuInSe_2$)=5.781 Å and *a*($CuIn_{1-x}Al_xSe_2$)=5.761 Å, as measured prior to and after post-selenisation treatment, respectively, and *a*($CuAlSe_2$)=5.606 Å, corresponding to the PDF file 00-044-1269. The tetragonal distortion of the CIS phase is in good agreement with the literature, where the Δ values (selected values are listed in reference [24]) generally vary between -0.008 and -0.010. Using equation (5) the values obtained are $x_{xrd}(a)$ = 0.11±0.03 or $x_{xrd}(c)$ = 0.08±0.01, depending on whether the *a* lattice parameter or the *c* lattice parameter is used for their determination, respectively.

GD-OES was performed on B4 after PSA and compared to the depth profiles performed after selenisation only (Figure 8). Note that softer plasma conditions and a smaller crater area were used for the measurement after PSA due to a reduced sample size. The two depth profiles show no significant difference, with increased Cu and Se signals at the front (region *a*), relatively constant signals through most of region *b*. A similar increase of the Al signal, in parallel with a decrease of Cu and In, is also observed near the interface with the Mo (end of

region *b*). The post-selenisation treatment did not yield any change in thickness when measured by stylus profilometry.

PSA therefore yielded incorporation of some of the aluminium into the CIS lattice of sample B4. This treatment did not, however, cause re-diffusion of Al from the back of the layer into the bulk, as GD-OES data (Figure 8) still shows segregation of Al at the back after PSA. It seems instead that Al was incorporated into the CIS lattice where Al was already present, that is near the Mo back contact. Some Al-free CIS was therefore left in the rest of the bulk.

4 Conclusion

Cu-In-Al thin films with four different x=[Al]/([Al]+[In]) ratios were selenised. Only for precursors with x>0.38 did the selenisation lead to some incorporation of the Al into the chalcopyrite lattice of $CuInSe_2$. Samples of content x=0.11 were selenised at temperatures ranging 250-540°C. XRD and PP-TOFMS analyses showed that the absence of CIAS originated in part from the Al segregation at the back of the film, at temperatures as low as 250°C. This is due to an excessive difference in temperature of formation between the binary selenides of In and that of Al_2Se_3. A post selenisation anneal at high temperature indicated a partial incorporation of Al into the CIS lattice and could be a new route towards fabricating single phase CIAS.

Acknowledgements

The authors acknowledge support of the UK Engineering and Physical Sciences Research Council SUPERGEN Initiative for the program ‘PV-21’.

References

[1] M.A. Green, K. Emery, Y. Hishikawa, W. Warta, E.D. Dunlop, Solar cell efficiency tables (version 39), Progress in Photovoltaics: Research and Applications, 20 (2012) 12-20.
[2] P.D. Paulson, M.W. Haimbodi, S. Marsillac, R.W. Birkmire, W.N. Shafarman, $CuIn_{1-x}Al_xSe_2$ thin films and solar cells, Journal of Applied Physics, 91 (2002) 10153-10156.
[3] T. Dullweber, U. Rau, M.A. Contreras, R. Noufi, H.W. Schock, Photogeneration and carrier recombination in graded gap $Cu(In,Ga)Se_2$ solar cells, IEEE Transactions on Electron Devices, 47 (2000) 2249-2254.
[4] S. Siebentritt, What limits the efficiency of chalcopyrite solar cells?, Solar Energy Materials and Solar Cells, 95 1471-1476.
[5] G. Hanna, A. Jasenek, U. Rau, H.W. Schock, Influence of the Ga-content on the bulk defect densities of $Cu(In,Ga)Se_2$, Thin Solid Films, 387 (2001) 71-73.
[6] I. Repins, M.A. Contreras, B. Egaas, C. DeHart, J. Scharf, C.L. Perkins, B. To, R. Noufi, 19.9%-efficient $ZnO/CdS/CuInGaSe_2$ solar cell with 81.2% fill factor, Progress in Photovoltaics, 16 (2008) 235-239.

[7] P. Jackson, D. Hariskos, E. Lotter, S. Paetel, R. Wuerz, R. Menner, W. Wischmann, M. Powalla, New world record efficiency for Cu(In,Ga)Se_2 thin-film solar cells beyond 20%, Progress in Photovoltaics: Research and Applications, 19 (2011) 894-897.
[8] S. Marsillac, P.D. Paulson, M.W. Haimbodi, R.W. Birkmire, W.N. Shafarman, High-efficiency solar cells based on Cu(InAl)Se_2 thin films, Applied Physics Letters, 81 (2002) 1350-1352.
[9] I. Bondar', A. Vaipolin, L. Unyarkha, Inorganic Materials, 21 (1985) 1447-1449.
[10] L. Palatnik, E. Belova, Inorganic Materials, 3 (1967) 865-870.
[11] Solar Frontier, Solar Frontier Sets New Efficiency World Record, *retrieved 29th February 2012*, http://www.solar-frontier.com/eng/news/2012/C002980.html.
[12] D. Dwyer, I. Repins, H. Efstathiadis, P. Haldar, Selenization of co-sputtered CuInAl precursor films, Solar Energy Materials and Solar Cells, 94 (2010) 598-605.
[13] R. Aninat, Study of Cu(In,Al)Se_2 thin films prepared by selenisation of sputtered metallic precursors for applications in solar cells, PhD thesis: Northumbria University 2012
[14] R. Klenk, R. Menner, D. Cahen, H.W. Schock, Improvement of Cu(Ga,In)Se_2 based solar cells by etching the absorber, in: proceedings of 21st IEEE Photovoltaic Specialists Conference, 1990, vol. 1, p.^pp. 481-486.
[15] D.G. Moon, J.H. Yun, J. Gwak, S. Ahn, A. Cho, K. Shin, K. Yoon, S. Ahn, Cu(In,Ga)Se_2 thin films without Ga segregation prepared by the single-step selenization of sputter deposited Cu-In-Ga-Se precursor layers, Energy & Environmental Science, 5 (2012) 9914-9921.
[16] J. Olejnícek, C.A. Kamler, S.A. Darveau, C.L. Exstrom, L.E. Slaymaker, A.R. Vandeventer, N.J. Ianno, R.J. Soukup, Formation of $CuIn_{1-x}Al_xSe_2$ thin films studied by Raman scattering, Thin Solid Films, 519 (2011) 5329-5334.
[17] R. Caballero, C. Guillén, $CuInSe_2$ Formation by selenization of sequentially evaporated metallic layers, Solar Energy Materials and Solar Cells, 86 (2005) 1-10.
[18] K.G. Reinsberg, C. Schumacher, A. Tempez, K. Nielsch, J.A.C. Broekaert, Depth-profile analysis of thermoelectric layers on Si wafers by pulsed r.f. glow discharge time-of-flight mass spectrometry, Spectrochimica Acta Part B: Atomic Spectroscopy, 76 (2012) 175-180.
[19] F. Hergert, R. Hock, A. Weber, M. Purwins, J. Palm, V. Probst, In situ investigation of the formation of Cu(In,Ga)Se_2 from selemsed metallic precursors by X-ray diffraction - The impact of Gallium, Sodium and Selenium excess, Journal of Physics and Chemistry of Solids, 66 (2005) 1903-1907.
[20] T. Do, N.S. McIntyre, Pressure effects on aluminium oxidation kinetics using X-ray photoelectron spectroscopy and parallel factor analysis, Surface Science, 440 (1999) 438-450.
[21] M. Marudachalam, R. Birkmire, J.M. Schultz, T. Yokimcus, Characterization of Cu-In-Ga precursors used to form Cu(In,Ga)Se_2 films, in: proceedings of 24th IEEE Photovoltaic Specialists Conference 1994, vol. 1, p.^pp. 234-237 vol.231.
[22] B.M. Basol, V.K. Kapur, A. Halani, C.R. Leidholm, J. Sharp, J.R. Sites, A. Swartzlander, R. Matson, H. Ullal, Cu(In,Ga)Se_2 thin films and solar cells prepared by selenization of metallic precursors, Journal of Vacuum Science & Technology a-Vacuum Surfaces and Films, 14 (1996) 2251-2256.
[23] S. Jost, F. Hergert, R. Hock, M. Purwins, R. Enderle, Real-time investigations of selenization reactions in the system Cu-In-Al-Se, physica status solidi (a), 203 (2006) 2581-2587.
[24] W. Paszkowicz, R. Lewandowska, R. Bacewicz, Rietveld refinement for $CuInSe_2$ and $CuIn_3Se_5$, Journal of Alloys and Compounds, 362 (2004) 241-247.

Table 1: Deposition and processing data for the samples presented. EDS compositions in italics are overall compositions including the Cu capping layer. They were extrapolated from the precursor composition and mass before capping, and the thickness of the Cu cap.

Table 2: Selenisation steps summary and phases detected in the XRD scans. * indicates phases found only in trace amounts or low crystallinity.

Table 3: EDS composition of B1, B2, B3 and B4. Note: B4 was analysed after a post-selenisation anneal at 573°C for 60 min without Se.

Table 4: Lattice parameters and tetragonal distortion of the different chalcopyrite phases observed in the XRD patterns before and after post-selenisation anneal, determined using EVA 10.0 software from Brüker AXS. The values of x_{xrd} determined from the lattice parameters of the CIAS phase are also reported.

Figure 1: XRD patterns of four selenised Cu-In-Al precursors, A1 (x_p=0.11, 530°C, 30 min dwell, 1000 Pa H_2/N_2), A2 (x_p=0.31, 530°C, 30 min, 1000 Pa H_2/N_2), A3 (x_p=0.38, 530°C, 30 min, 1000 Pa H_2/N_2) and A4 (x_p=0.51, 540°C, 30 min, 1000 Pa Ar).

Figure 2: XRD patterns of A3' and A3, made of identical precursors (x_p=0.38) and selenised together (530°C, 30 min, 1000 Pa H_2/N_2).

Figure 3: GD-OES depth profiles of A3 (x_p=0.38, 530°C, 30 min, 1000 Pa H_2/N_2). For clarity of the figure, the Se signal was amplified and the Mo signal decreased.

Figure 4: WDS/EDS linescan (a) performed along the cross section of A3' (x_p=0.38, 530°C, 30 min, 1000 Pa H_2/N_2). Next to each element is indicated the detection technique used. The linescan is shown on the SEM micrograph of the cross section (b).

Figure 5: XRD patterns of samples B1, B2, B3 and B4 after selenisation. The low crystallinity phases In and α-In_2Se_3 are not marked on the graphs for clarity but are reported in Table 2.

Figure 6: PP-TOFMS depth profiles of B1 (130°C-250°C), B2 (130°C-250°C-350°C), B3 (130°C-250°C-450°C) and B4 (130°C-250°C-540°C). The Al profile is zoomed on in the inset graphs. The regions defined (a, b and c) are discussed in the body of the text.

Figure 7: XRD patterns of sample B4 before (black line) and after (red line) 1h post-selenisation anneal (573°C, 60 min, 1000 Pa Ar). In the inset the Mo (110) reflection is shown. The absence of significant shift for this reflection rules out important lattice strain in the film.

Figure 8: GD-OES depth profiles of B4 before (*top*) and after (*bottom*) 60 min anneal without Se. The signal intensities and the sputtering time were normalised to the Mo signal for the comparison of the two graphs.

ID	Layout	Comp. (at%)			Se?	Gas	Pressure (Pa)	Dwell Temperature (°C)	Dwell duration (min.)	Ramp duration (min.)
		Cu	In	Al						
A1	Cu-In-Al	46.0	48.0	6.0	Yes	H_2/N_2	1000	530	30	≈30
A2	Cu-In-Al	48.0	38.0	14.0	Yes	H_2/N_2	1000	530	30	≈30
A3	Cu-In-Al	49.0	31.5	19.5	Yes	H_2/N_2	1000	530	30	≈30
A4	Cu-In-Al	48.0	25.0	27.0	Yes	Ar	1000	540	30	≈30
A3'	Cu-In-Al	49.0	31.5	19.5	Yes	H_2/N_2	1000	530	30	≈30
B1	Cu-In-Al/Cu	*62.0*	*33.8*	*4.2*	Yes	Ar	600	130-250	30 (x2)	≈13
B2	Cu-In-Al/Cu	*62.0*	*33.8*	*4.2*	Yes	Ar	600	130-250-350	30 (x3)	≈20
B3	Cu-In-Al/Cu	*62.0*	*33.8*	*4.2*	Yes	Ar	600	130-250-450	30 (x3)	≈25
B4	Cu-In-Al/Cu	*62.0*	*33.8*	*4.2*	Yes	Ar	600	130-250-530	30 (x3)	≈30
					No*	Ar	1000	573	60	≈30

*Post-selenisation anneal

ID	Step 1	Step 2	Step 3	**XRD phases**
B1	130°C	250°C	-	$Cu_{0.938}InSe_2$*, $Cu_{2-x}Se$, $CuSe_2$, In_4Se_3, α-In_2Se_3*, $Cu_{16}In_9$*
B2	130°C	250°C	350°C	$Cu_{2-x}Se$, $Cu_{0.938}InSe_2$, $Cu_{16}In_9$*, In*
B3	130°C	250°C	450°C	$Cu_{2-x}Se$, $Cu_{0.938}InSe_2$, $Cu_{16}In_9$*, In*
B4	130°C	250°C	540°C	$Cu_{2-x}Se$, $Cu_{0.938}InSe_2$

* Traces or low crystallinity

ID	EDS composition (at %)						Cu/ (Al+In)	Al/ (Al+In)	Se/ (Al+In)
	Cu	In	Al	Se	Mo	O			
B1	28.3	1.8	2.9	66.7	0.0	0.4	6.09	0.62	14.33
B2	34.1	17.8	2.9	44.1	0.8	0.3	1.65	0.14	2.14
B3	25.0	22.3	2.2	45.7	0.3	4.4	1.02	0.09	1.86
B4	26.8	21.2	2.3	40.5	3.0	6.2	1.14	0.10	1.72

Process	Peak	a (Å)	c (Å)	Δ=2-c/a	x_{xrd}= [Al]/([Al]+[In])
Selenisation	CIS	5.781±0.004	11.612±0.008	-0.009±0.003	*NA*
	CIAS	*NA*	*NA*	*NA*	*NA*
Selenisation+PSA	CIS	5.783±0.01 (1)	11.612±0.008	-0.008±0.005	*NA*
	CIAS	5.761±0.004	11.558±0.008	-0.006±0.003	0.08±0.01 (***from c***) 0.11±0.03 (***from a***)

(1) Due to the low intensity of the (312) CIS peak, the (112) reflection was used to determine *a*, yielding a more important error.

Figure 1

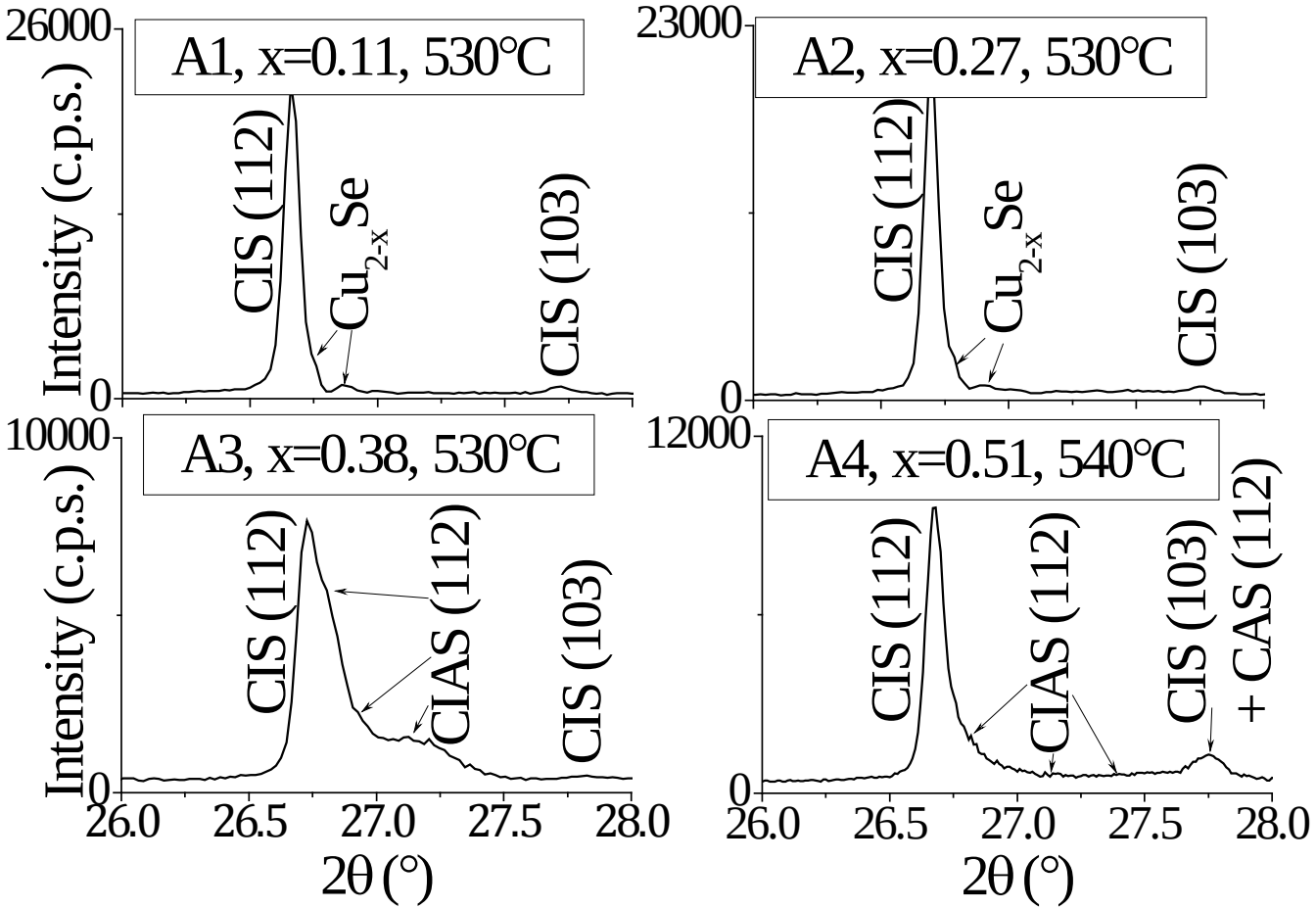
A1, x=0.11, 530°C
A2, x=0.27, 530°C
A3, x=0.38, 530°C
A4, x=0.51, 540°C
Intensity (c.p.s.)
2θ (°)
CIS (112)
Cu2-xSe
CIS (103)
CIAS (112)
+ CAS (112)
26000
23000
10000
12000
0
26.0
26.5
27.0
27.5
28.0

Figure 2

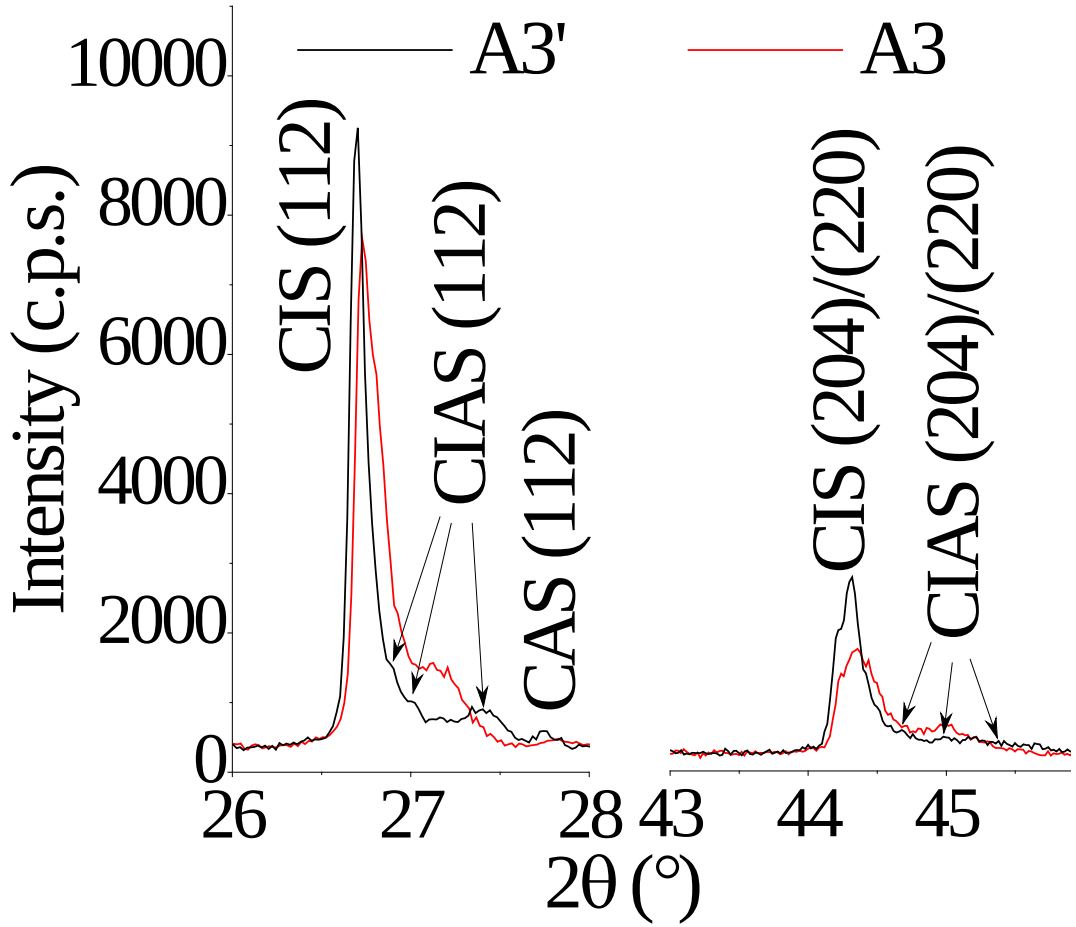
A3'
A3
Intensity (c.p.s.)
10000
8000
6000
4000
2000
0
CIS (112)
CIAS (112)
CAS (112)
CIS (204)/(220)
CIAS (204)/(220)
26
27
28
43
44
45
2θ (°)

Figure 3

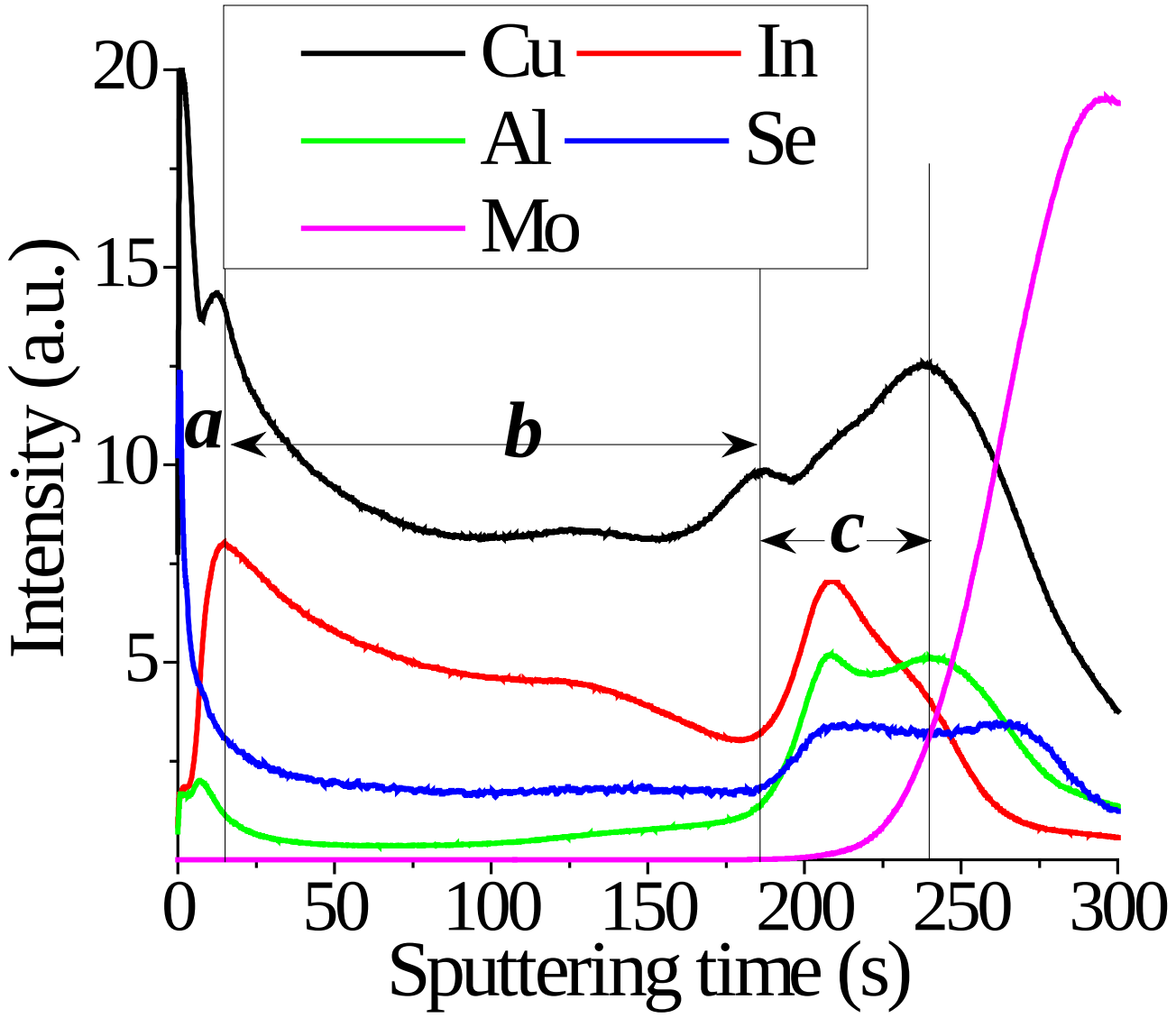
Cu
In
Al
Se
Mo
a
b
c
Intensity (a.u.)
Sputtering time (s)
0
50
100
150
200
250
300
5
10
15
20

Figure 4

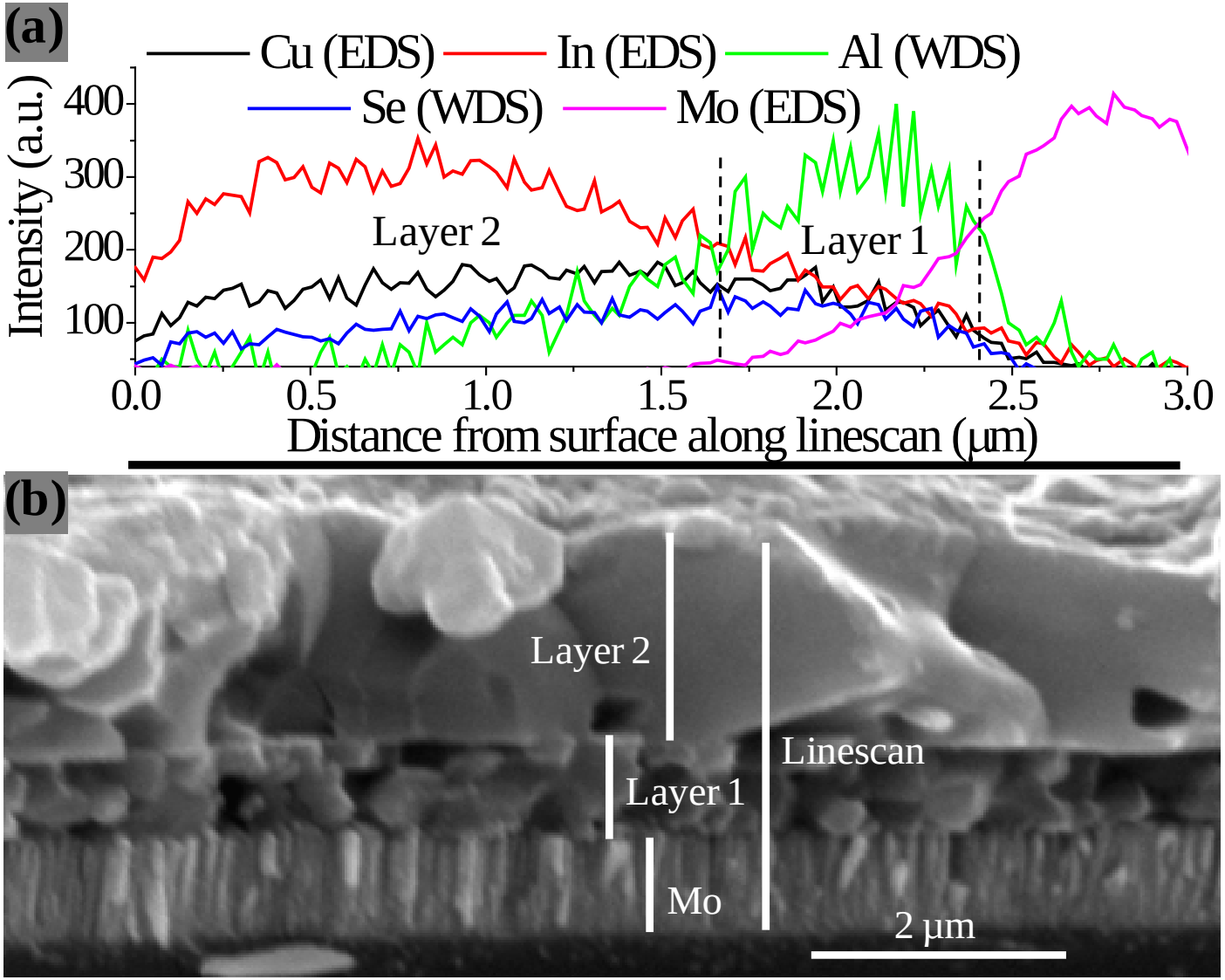
(a)
Cu (EDS)
In (EDS)
Al (WDS)
Se (WDS)
Mo (EDS)
Intensity (a.u.)
400
300
200
100
Layer 2
Layer 1
0.0
0.5
1.0
1.5
2.0
2.5
3.0
Distance from surface along linescan (µm)
(b)
Layer 2
Layer 1
Mo
Linescan
2 µm

Figure 5

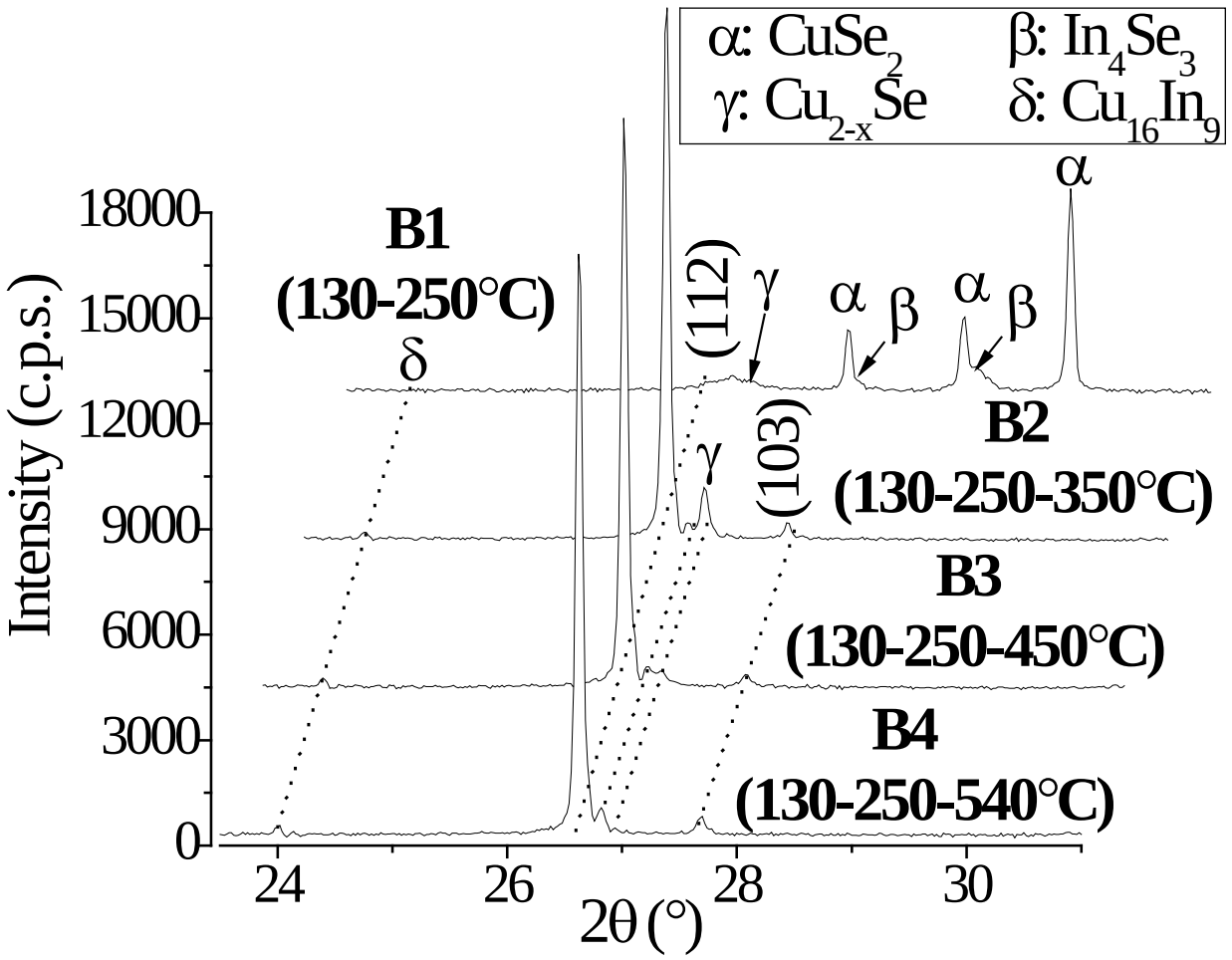
α: CuSe2
β: In4Se3
γ: Cu2-xSe
δ: Cu16In9
B1
(130-250°C)
B2
(130-250-350°C)
B3
(130-250-450°C)
B4
(130-250-540°C)
(112)
(103)
Intensity (c.p.s.)
2θ (°)
18000
15000
12000
9000
6000
3000
0
24
26
28
30

Figure 6

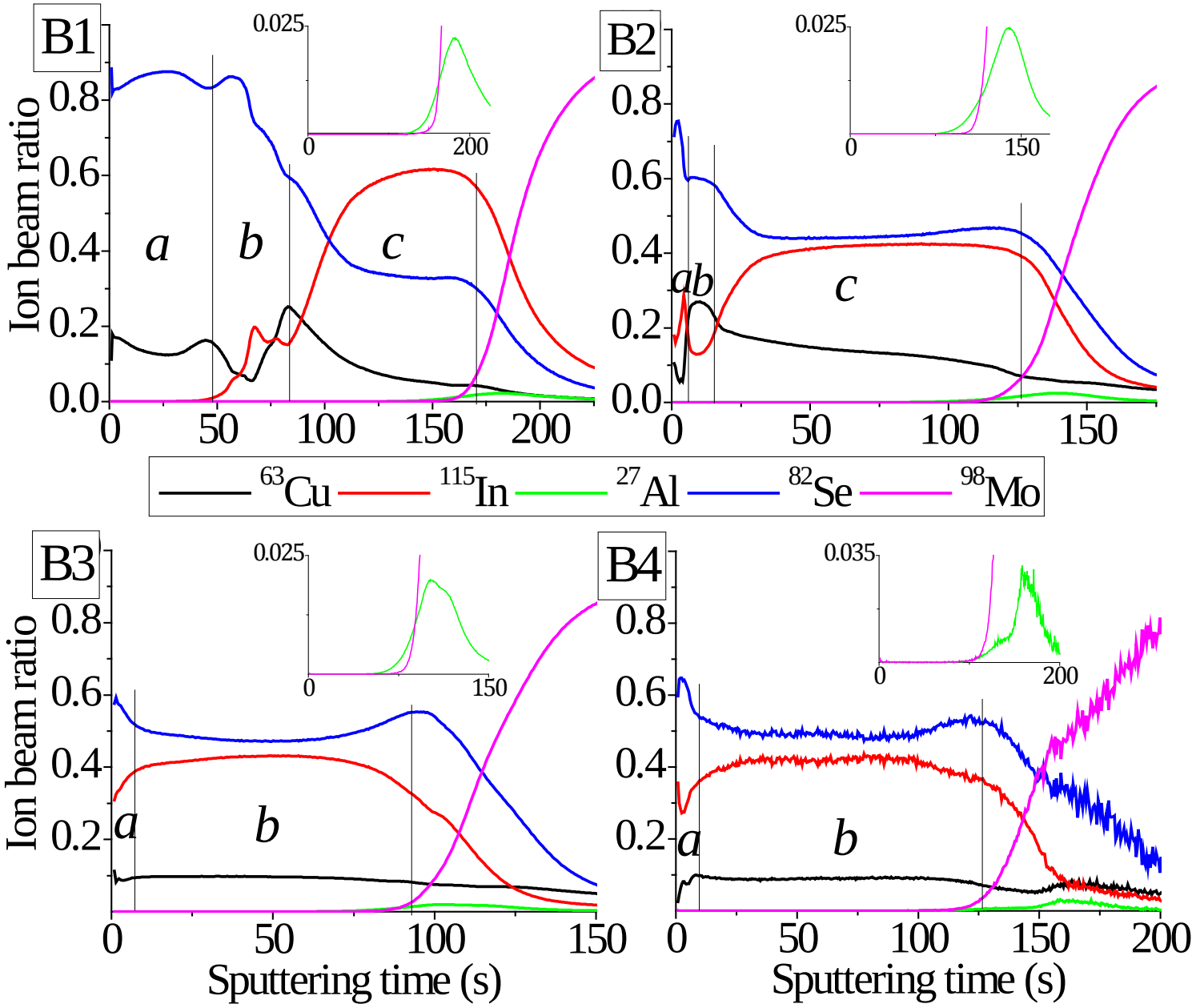
B1
B2
B3
B4
Ion beam ratio
Sputtering time (s)
a
b
c
ab
0.025
0.035
0
200
150
0.0
0.2
0.4
0.6
0.8
0
50
100
150
200
63Cu
115In
27Al
82Se
98Mo

Figure 7

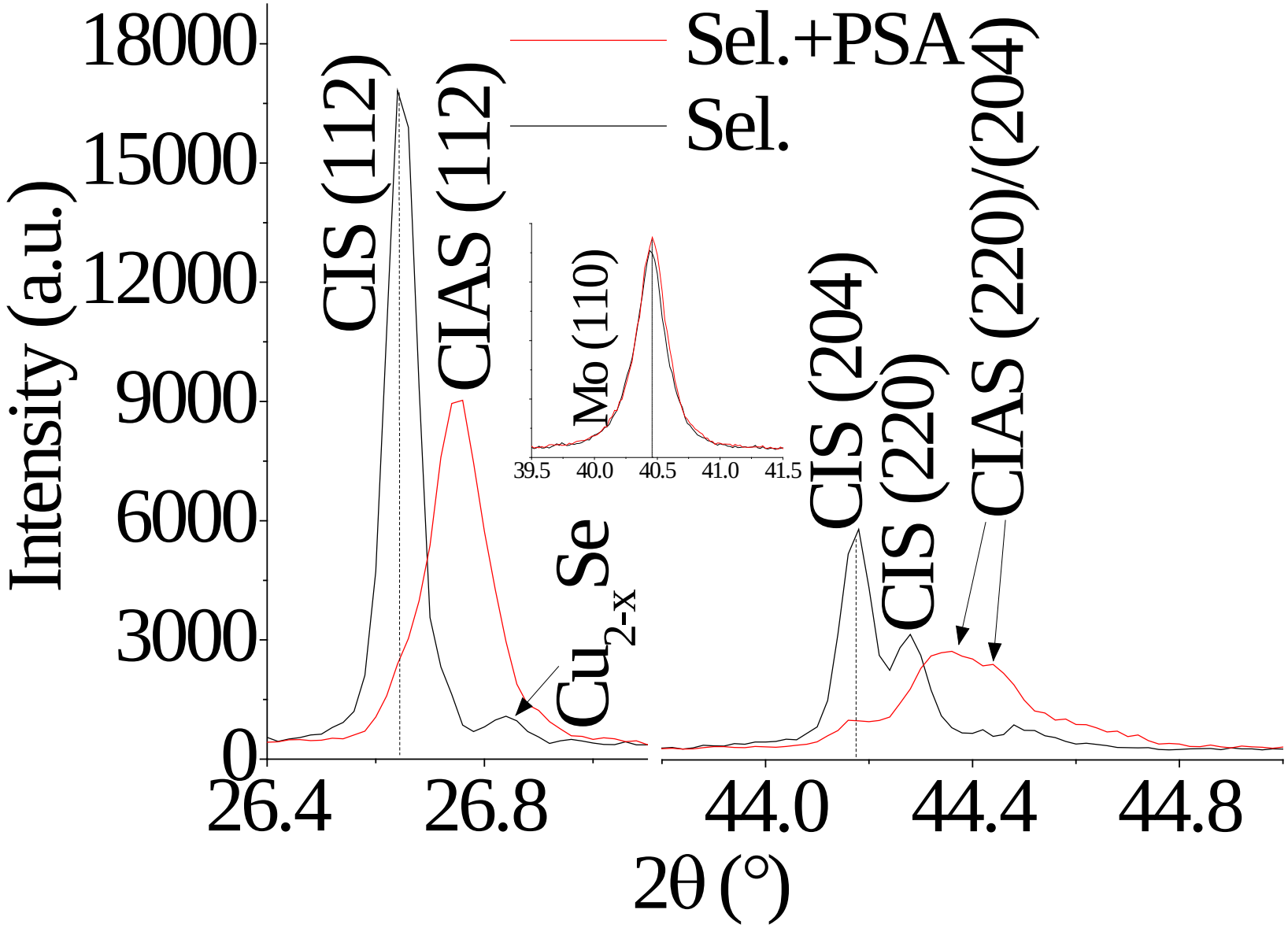
Sel.+PSA
Sel.
Intensity (a.u.)
18000
15000
12000
9000
6000
3000
0
CIS (112)
CIAS (112)
Mo (110)
39.5
40.0
40.5
41.0
41.5
Cu2-xSe
CIS (204)
CIS (220)
CIAS (220)/(204)
26.4
26.8
44.0
44.4
44.8
2θ (°)

Figure 8

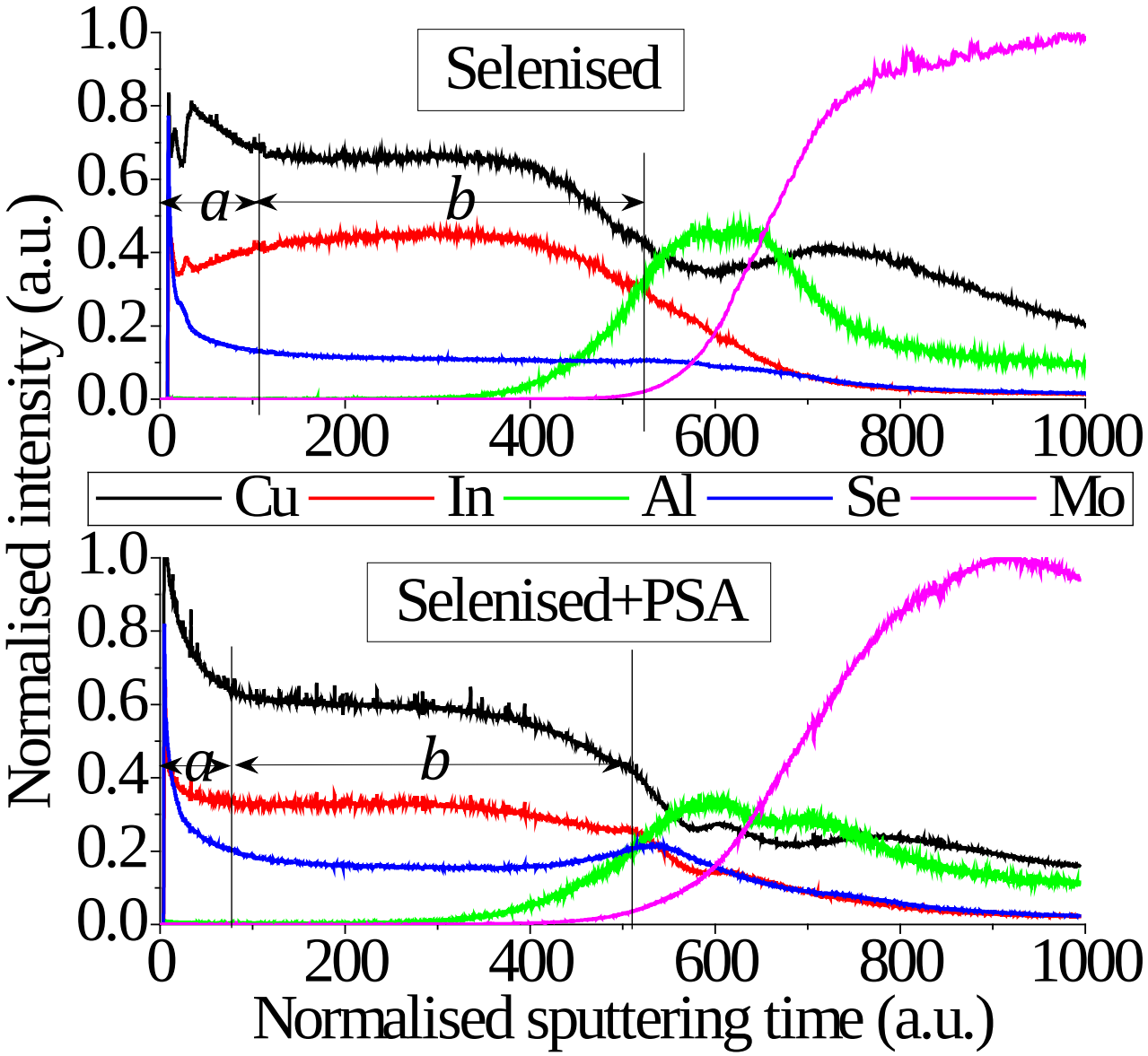
Selenised
Selenised+PSA
a
b
Cu
In
Al
Se
Mo
Normalised intensity (a.u.)
Normalised sputtering time (a.u.)
0.0
0.2
0.4
0.6
0.8
1.0
0
200
400
600
800
1000